Available online at www.sciencedirect.com
SCIENCE DIRECT®
Journal of Nuclear Materials 323 (2003) 229–242
journal of nuclear materials
www.elsevier.com/locate/jnucmat

Helium accumulation in metals during irradiation – where do we stand?

H. Trinkaus [a,*], B.N. Singh [b]

[a] ESS-Projekt, Forschungszentrum Jülich, Institut für Festkorperforschung, D-52425 Jülich, Germany
[b] Materials Research Department, Risø National Laboratory, DK 4000 Roskilde, Denmark

Abstract

In the present contribution, the basic ideas pertinent to modelling helium accumulation in metals are reviewed. Topics of earlier work are: Diffusion of atomic He and bubble nucleation under irradiation, low temperature (diffusion controlled) vs. high temperature (dissociation controlled) nucleation, cascade induced He resolution and continuous bubble nucleation at high doses, homogeneous in the bulk vs. heterogeneous nucleation at extended defects; bubble coarsening upon annealing, migration and coalescence vs. Ostwald ripening; bubble state, upper limit vs. 'equilibrium' pressure, high pressure equation of state of He, bubble-to-void transformation under a stress or irradiation induced effective vacancy supersaturation. More recent topics are: formation and growth limitation of He platelets (He-filled nano-cracks) in some metals and ceramics, coupled two-component Ostwald ripening of bubble–loop complexes. Possible effects of bubble formation on mechanical properties are briefly addressed: hardening and embrittlement, particularly at high temperature where intergranular fracture is induced by the transformation of bubbles to voids at grain boundaries. Finally, important but unsolved problems are identified and their relevance are briefly discussed.

PACS: 61.82.Bg; 61.80.Az; 61.72.Qq; 62.20.Mk

1. Introduction

Macroscopic radiation damage effects in structural components of nuclear devices such as fission or fusion reactors are the consequence of two fundamentally different types of interactions between the projectile particles of the irradiation and the atoms of the material under irradiation: atomic displacements resulting in vacancy and self-interstitial type lattice defects, and nuclear reactions creating foreign elements [1]. The creation of helium atoms in metals is considered with particular concern since their precipitation into bubbles can substantially deteriorate mechanical material properties, particularly in metals at high (homologous) temperatures, $T \geqslant 0.5T_m$ (T_m: melting temperature), where drastic embrittlement of metals due to helium bubbles formation at grain boundaries has been found to occur even at very low overall helium concentrations [1–3].

In view of this, it is understandable that, starting with the basic work by Greenwood et al. [4], effects of He in metals have been modeled in the past in many groups all over the world, in the USA, for instance, at the UCSB, at UCLA, at ORNL, in Europe at Harwell and Risø, at FZ Jülich, at PSI, in Russia at Kurchatov Institute.

The basic problem is that the understanding of macroscopic effects due to He accumulation requires modelling at many different levels, from atomic properties of He atoms in metal lattices such as He atom configurations and the corresponding energies, over diffusion mechanisms, kinetics of bubble nucleation and growth to the relation between the microstructural evolution and the change in mechanical properties. We refer in this context to the proceedings on fundamental

* Corresponding author. Tel.: +49-2461 61 6460; fax: +49-2461 61 2620.
E-mail address: h.trinkaus@fz-juelich.de (H. Trinkaus).

0022-3115/$ - see front matter © 2003 Elsevier B.V. All rights reserved.
doi:10.1016/j.jnucmat.2003.09.001

aspect of helium in metals [5] and, more generally, on fundamental aspect of inert gases in solids [6].

In the present contribution, crucial ideas on modelling helium accumulation in metals and its effects on mechanical properties are reviewed. Most of these ideas originate from attempts to describe experimental observations analytically. We do not claim to present by the present contribution a general review of the whole topics but focus on previous own work and closely related other work. Section 2 deals with diffusion of He atoms. The main ideas concerning bubble formation under He production, and its dependence on temperature, He production rate and displacement rate, are presented in Section 3. Section 4 is devoted to bubble evolution during annealing. In Section 5, limiting cases of the thermodynamic state of He in cavities (bubbles/voids) are discussed. Unusual bubble features, such as He platelets and complexes of bubble and dislocation loops and possibilities to explain them are briefly described in Section 6. In Section 7, possible effects of bubble formation in metals on their mechanical properties are addressed. In a final section, 'where do we stand?', the present state of art in He accumulation in metals is discussed.

2. Helium diffusion

Because of its extremely low solubility in metals, helium occurs in metals only when it is forced in there, for instance by tritium decay, α-injection or by (n,α) reactions of neutrons with matrix nuclei during neutron irradiation. Hence, the accumulation of He in metals is always accompanied at least by some displacement damage, depending mainly on the ratio of the He production rate to the displacement rate.

Helium diffusion is a basic requirement for bubble nucleation and growth. It is the result of random jumps of He atoms from one to another (meta-)stable lattice site. In Fig. 1, the most important types of lattice sites and migration modes for He atoms in metals at negligible radiation damage or during irradiation are illustrated. The most important positions for He atoms in a lattice are interstitial and substitutional sites (He atom in a vacancy). The preferential position and the dominant migration mode depend on temperature as well as on the presence of other intrinsic or irradiation induced defects acting as traps for He atoms, particularly in the presence of vacancies and He–vacancy clusters. Because of the strong binding of He atoms to vacancies (with energies of a few eV), the substitutional site is the preferential one if the vacancy concentration is significant. In He diffusion, He interstitial migration, vacancy migration and the removal of a He atom from a vacancy or a He–vacancy cluster by thermal activation or some athermal mechanism are the most important basic processes.

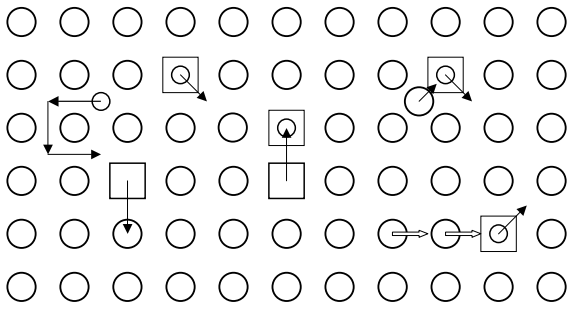

Fig. 1. Schematic illustration of defect configurations and jump processes relevant for He diffusion without and with irradiation. From left to right: migrating He interstitial, migrating vacancy, transformation of a substitutional to an interstitial He atom by thermally activated dissociation from its vacancy, jump of a He atom from one to another vacancy as a basic step in the vacancy mechanism, transformation of a substitutional to an interstitial He atom due to its replacement by a SIA, collisional displacement of a He atom.

2.1. Helium diffusion at negligible radiation damage [7]

(1) Interstitial migration: He atoms on interstitial sites diffuse interstitially, generally fast even below room temperature (with an activation energy of a few tenths of an eV), until they are trapped by another defect. Consequently, He diffusion is effectively of interstitial type over a spatial scale where the concentration (sink strength) of defects trapping He atoms is negligibly small. This condition is best realised in the case of He production by tritium decay in tritided (but otherwise pure) metals at $T < 0.5T_m$ where both the displacement damage and the concentration of thermal vacancies are small.

At temperatures $T > 0.5T_m$ interstitially diffusing He atoms will be mainly trapped by thermal vacancies. In this case, two different types of mechanisms contribute to He diffusion:

(2) The common 'vacancy mechanism' where a transient di-vacancy–He-complex is formed in which the He atom jumps from one to the other vacancy, and

(3) the 'impeded interstitial migration' or 'He–vacancy dissociation (dissociative) mechanism' where a He atom diffuses interstitially between its thermal dissociation from one vacancy and its re-trapping by another vacancy [7,8].

Mechanisms (2) and (3) are cooperative, meaning that the faster mechanism is the dominant one (for more details see Table 1). It is worth adding here that dislocations and grain boundaries (GBs) generally represent fast diffusion paths for He atoms.

2.2. Helium diffusion during irradiation

For He diffusion under irradiation, atomic displacements and the resulting vacancies, self-interstitial atoms

Table 1
Characterisation of helium diffusion mechanisms

Irradiation	He diffusion					
	Without [7]			With [8–10]		
T/T_m	<0.5	>0.5	>0.5	<0.2	>0.2, <0.5	~0.5
Mechanism	Interstitial	Vacancy	Dissociation	Displacement	Replacement	Vacancy
Diffusivity	D^m_{HeI}	$\sim D_v c_v^{th}$		D^{mix}	$\sim D_v$	$\sim D_v c_v$
Act. energy	E_{HeI}	$\sim E^{sd}$	$E^{diss}_{He,v} - E^f_v$	~0	$\sim E^m_v$	$\sim E^m_v/2$
Examples[a]	Tritides?	Al, Ag, Au, Ti?	Ti? Mg, V, Fe, Co, Ni, Cu, Mo, W	All metals?		

Symbols: D_{HeI}, D_v and D^{mix} are the diffusion coefficients of He interstitial atoms, of vacancies and for cascade mixing, respectively, E^m_{HeI}, E^m_v, E^f_v, E^{sd} and $E^{diss}_{He,v}$ are the activation energies for He interstitial diffusion, vacancy migration, vacancy formation, self-diffusion, He–vacancy dissociation, respectively (ordered according to their estimated magnitude), and $c_v^{(th)}$ is the (thermal) vacancy concentration.
[a] Question mark behind examples indicates that mechanism is not (uniquely) verified experimentally.

(SIAs) and clusters of these defects play a crucial role. The following mechanisms may be distinguished [8–10]:

(I) The athermal 'displacement or cascade mixing mechanism' where He diffusion is due to direct displacements. This mechanism is expected to be dominant below annealing stage III where vacancies are immobile (at $T < 0.2T_m$).

(II) The 'replacement mechanism' where a He atom diffuses interstitially between its athermal replacement from a vacancy by a SIA and its re-trapping by another vacancy. This is likely to be the dominant mechanism between $0.2T_m$ and $0.5T_m$.

(III) The radiation enhanced 'vacancy mechanism' [10] which can dominate the 'replacement mechanism' only at temperatures around and above $0.5T_m$.

Mechanisms (I) to (III) are cooperative, meaning that the fastest mechanism is the dominant one (for more details see Table 1).

It is emphasised here that the exact mechanism controlling He diffusion has been identified experimentally by thermal absorption spectroscopy only for high temperatures and at negligible radiation damage, and even in this parameter range only for a restricted number of metals [7].

3. Bubble nucleation during He production

3.1. General features

The most important parameters controlling the number density and size of bubbles evolving during He production by implantation or transmutation are temperature, He production rate, displacement rate and accumulated He concentration (dose or time). For well annealed (homogeneous) metals and alloys, transmission electron microscopy (TEM) implanted with He (or irradiated with neutrons at concurrent He production) at elevated temperature has revealed the following main features [11]:

(1) At a given temperature (and low displacement doses <1 dpa), the bubble density seems not to depend significantly on He concentration or time while the average bubble size increases continuously when bubbles become visible in TEM, indicating that bubble nucleation has occurred in an early stage and virtually ceased afterwards.

(2) The temperature dependence of apparently saturated bubble densities exhibits two clearly discernible branches, one at low and the other at high temperature, characterized by low and high apparent activation energies, respectively (Fig. 2).

(3) At a given temperature and accumulated He concentration, experimental data indicate, in spite of a considerable amount of scatter, that bubble densities and sizes increase and decrease, respectively, with increasing He production rate.

Absolute values of the observed bubble densities range from maximum values of the order of 10^{25} m^{-3} at temperatures around and below stage III ($T < 0.2T_m$) down to the limit of quantitative TEM data ($\approx 10^{18}$ m^{-3}) at temperatures above stage V ($T > 0.5T_m$). Modelling bubble nucleation means explaining both the qualitative features as well as the quantitative values.

3.2. Low temperature vs. high temperature nucleation

Under the condition of He production and displacement damage, the nucleation of He bubbles within grains of a metal matrix occurs by the concurrent diffusion and clustering of He atoms, vacancies (and SIAs). Bubble nucleation thus represents a generally complicated multi (at least two)-component nucleation process. The theoretical tools to treat this are rate theory, the Fokker–Planck approach or some form of 'classical' nucleation theory for varying effective supersaturations of He atoms and vacancies.

The treatment simplifies when the vacancy-SIA component plays a minor role in bubble nucleation compared to that of He, or is even 'enslaved' by the He

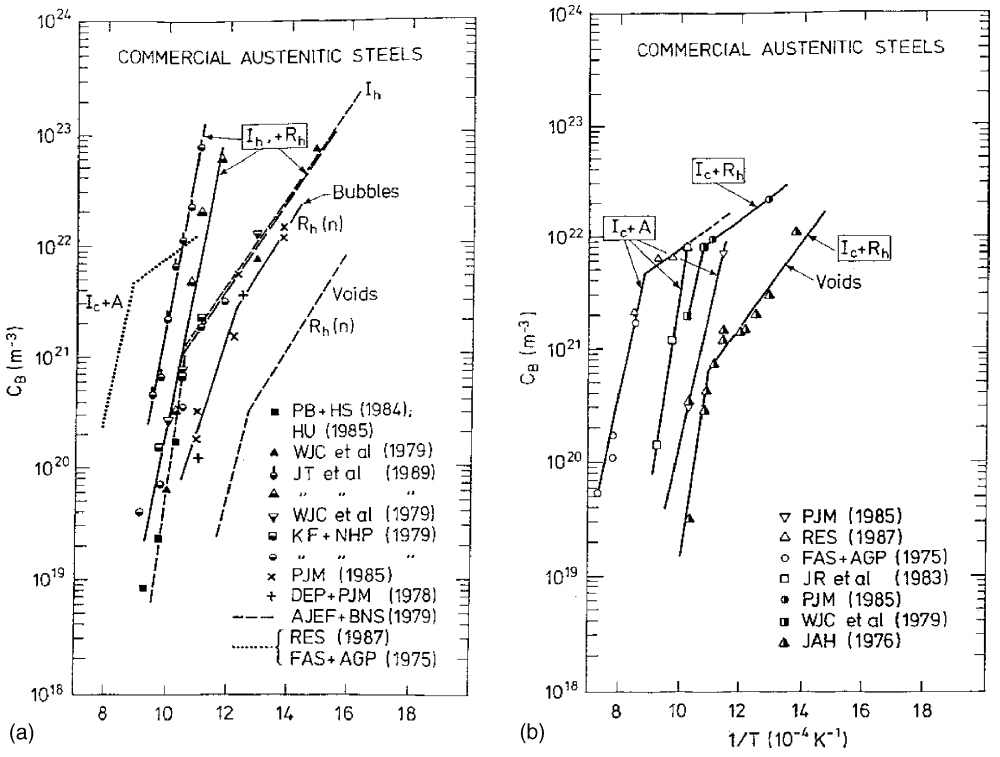

Fig. 2. Temperature dependence of observed densities of bubbles formed in commercial austenitic steels (a) during implantation/irradiation at elevated temperatures ('hot implantation/irradiation', I_h/R_h), (b) during annealing after pre-implantation/irradiation at low temperatures ('cold implantation/irradiation' followed by annealing, $I_c + A/I_c + R_h$). Note the high and low temperature branches. The symbols and related capital letters refer to authors [12].

component. This is expected to hold at relatively high ratios of He production to displacement rates and at temperatures above stage V ($T > 0.5T_m$).

In such cases, the characteristic features of bubble nucleation during He production at low displacement doses may be illustrated by schematic plots of the relevant quantities vs. time as shown in Fig. 3 [12,13]. These features are governed by the strong dependence of the nucleation rate, i.e. the temporal change of the number density of stable bubble nuclei, dN/dt, on the time-dependent concentration of He atoms in 'solution', $c(t)$, and the increasing absorption rate of these by the increasing number density of bubble nuclei, N. Accordingly, dN/dt increases strongly with increasing c at the beginning, but both quantities pass maxima, say at $t = t^*$, when production and absorption rates of He atoms balance each other approximately,

$$P \propto Dc^*N^*. \tag{1}$$

Thus, the nucleation process is characterized by 'self-limitation'. After the nucleation peak, both the nucleation rate, dN/dt, and the He concentration, c, decrease, the former much more strongly, however, than the latter, while the density, N, virtually saturates, and the average size, r, increases continuously due to absorption of newly produced He.

The bubble density nucleated during the whole nucleation peak is about 2–3 times that at the peak maximum, $N(t \gg t^*) \sim (2\text{–}3)N^*$. Eq. (1) in combination with estimates for the maximum He concentration c^* for two limiting cases representative of bubble nucleation at low and high temperatures, respectively, have been used to estimate $N(t \gg t^*)$ [12,13].

In the 'di-atomic nucleation' model where already two He atoms are assumed to form a stable bubble nucleus, the maximum nucleation rate is reached when a newly created He atom is as likely to reach an existing nucleus as to meet another He atom, i.e. when the concentrations of bubble and He atoms are comparable [4,12,13]. Using this, $c^* \propto N^*$, Eq. (1) yields the relation

$$N(t \gg t^*) \sim (2\text{–}3)N^* \propto (P/D)^{1/2}. \tag{2}$$

According to Eq. (2), the low T di-atomic nucleation may be characterised as being 'He diffusion controlled', with the He diffusion constant representing the key material parameter. The apparent activation energy of

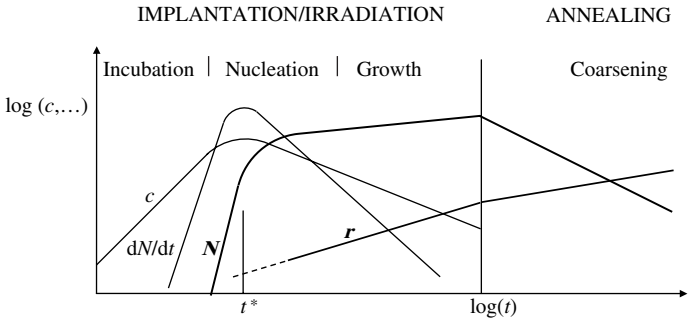

Fig. 3. Schematic representation of the time-dependence of the main quantities characterising bubble nucleation during He production and bubble coarsening during annealing: He atoms in 'solution', c, nucleation rate, dN/dt, density, N, and average size, r, of nucleated bubbles. A double-log representation is used to indicate by straight line segments approximate power law behaviour where applicable. Note the strongly peaked nucleation rate and the approximate saturation of N during He production and the decrease of the density at a simultaneous decrease of the size of bubbles during annealing.

the bubble density N is (minus) half of the He diffusion energy. For He diffusion by the replacement mechanism, this would be $\sim E_v^m/2$ (see Table 1) in qualitative agreement with trends deduced from TEM data for bubble densities [11]. Concerning the predicted square root dependence, $N \propto P^{1/2}$, a similar qualitative agreement with experimental data is found [11].

Inclusion of bubble migration by surface diffusion (with diffusion coefficient $\sim D_v$) does not change the predicted general trends even though it reduces the absolute values of N [10,12,14]. Estimates of such absolute values on the basis of this range from orders of 10^{25} m^{-3} down to 10^{21} m^{-3} at $0.2T_m$ and $0.5T_m$, respectively, again in order of magnitude agreement with TEM data.

At high temperatures, small He (–vacancy) clusters can no longer be considered to be thermally stable. Only clusters above some critical size, depending via $c(t)$ on time, are stabilized by the available supply of He atoms. In this 'multi-atomic' nucleation, the nucleation rate becomes significant only around some critical atomic He concentration c^* in solution, which may now be interpreted as the thermal equilibrium He concentration in the presence of critical clusters of minimum size during the nucleation peak. Thus, Eq. (1) yields the relation [12,13]

$$N(t \gg t^*) \propto P/Dc^*. \tag{3}$$

Since Dc^* in Eq. (3) is a measure for thermal He re-solution (dissociation) from critical nuclei, the high T multi-atomic nucleation may be characterised as being 'He re-solution or dissociation controlled'. Accordingly, in this case, the apparent activation energy of N is equal to (minus) the energy for He re-solution (dissociation) from critical nuclei which thus would represent a key parameter in high T bubble nucleation. TEM data for bubble densities at high T (such as shown in Fig. 2) indicate values for this activation energy around the self-diffusion energy which appears reasonable.

The linear dependence of N on P suggested by Eq. (3) can be tested by normalizing available high temperature data for a certain metal to the He production rate used in the experiments. This has been done for commercial stainless steels as shown in Fig. 4. The condensation of the widely scattered original data by this normalisation into a rather narrow band confirms the linear rate dependence suggested by Eq. (3) [11].

With increasing ratio of the displacement to He production rate, the vacancy-SIA component becomes increasingly more important in bubble nucleation, which then has to be treated adequately as a multi-component nucleation process. The parameter set where the transition from an effectively one- to multi-component nucleation occurs are presently not clear, and the multi-component bubble nucleation process under concurrent He atom and displacement generation is even less clear. Numerical procedures to deal with bubble nucleation under general irradiation conditions are in progress [15].

3.3. Cascade induced He resolution and secondary bubble nucleation

The description of bubble nucleation given in the preceding sections 3.1 and 3.2 is only valid for low total (implanted or generated) He concentration and/or low displacement dose where the dynamic re-solution of He atoms from existing bubbles by displacement cascades is negligible compared to the implantation or generation of further He atoms. Some experiments, where He was implanted into metals at intermediate temperatures (between $0.2T_m$ and $0.5T_m$) to relatively high concentrations and simultaneously or subsequently irradiated to high doses, provide clear evidence that He atoms are

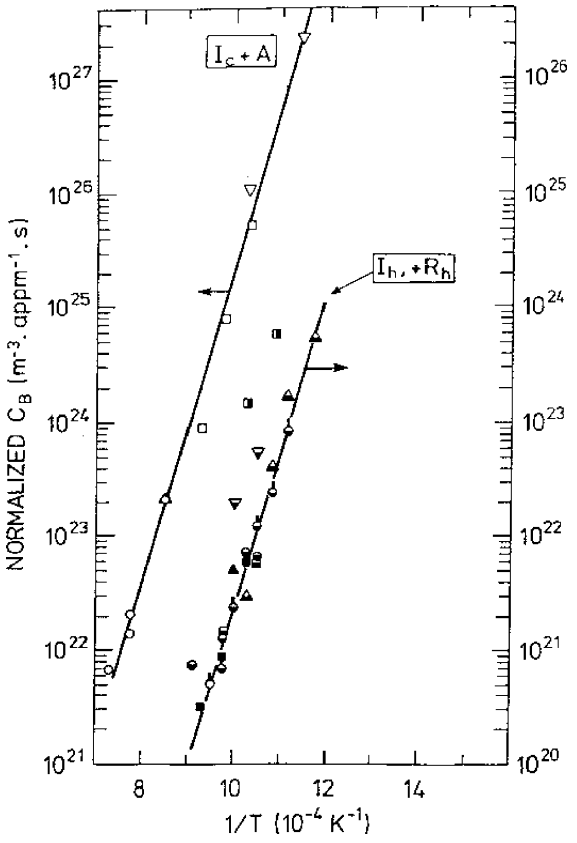

Fig. 4. Temperature dependence of bubble densities normalised to a He production rate and a ratio of He concentration to annealing time of 1 appm/s, for 'hot implantation/irradiation' and 'cold implantation/ irradiation' followed by annealing, respectively, using square root relations for the low temperature and linear relations for the high temperature regimes. Note the condensation of data points in comparison to Fig. 2, particularly at high temperature.

rather effectively resolved from small bubbles by displacement cascades resulting in the nucleation of secondary generations of bubbles [16]. The details of the resolution process and its high efficiency are presently not understood.

The problem of He resolution from bubbles and secondary bubble nucleation was discussed previously [17,18]. Recently, a simple analytical model, assuming that a certain fraction of He atoms in a bubble (characterised by a resolution parameter, κ) is resolved per dpa and that bubble nucleation occurs by the di-atomic nucleation mechanism described in Section 3.2, was presented [19], yielding for high doses above about 1 dpa a linear increase in the bubble density with dose at constant bubble size (see Fig. 5):

$$N \propto (P/D)^{3/7}(P/\kappa K)^{1/7}\kappa Kt, \tag{4a}$$

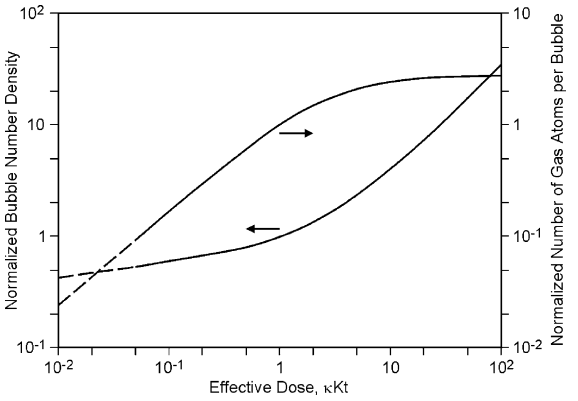

Fig. 5. Bubble density and average number of gas atoms per bubble, normalised to their values at $\kappa Kt = 1$, vs. the 'effective dose' κKt. For $\kappa Kt \ll 1$ (left), the lines are broken to indicate that they are valid only beyond the primary nucleation peak.

$$R \propto (DP/\kappa^2 K^2)^{1/7}. \tag{4b}$$

According to Eqs. (4a,b), at high doses, bubble density and size do not only depend on the primary gas production rate, P, but even stronger on the displacement rate K. Both depend, via $D(T)$, only weakly on temperature.

The applicability of models of this type seems to be restricted to the temperature range $0.2T_m < T < 0.5T_m$ corresponding to the fact that significant effects of cascade induced He resolution on bubble formation have only been observed in that range. This may be rationalised in the following way. Below $0.2T_m$ (where He diffuses by the displacement mechanism), primary and secondary bubble nucleation become indiscernible and bubble nuclei formed do not exceed sizes of atomic scale (He–vacancy clusters containing up to a few tens of He atoms). Above $0.5T_m$ He atom resolution becomes increasingly inefficient with increasing temperature ($\kappa \to 0$) because of the increasing re-absorption of resolved He atoms by bubbles of increasing size, while, on the other hand, thermal dissociation of gas atoms from bubble nuclei becomes the dominant mechanism.

3.4. Homogeneous vs. heterogeneous nucleation

In the preceding section, possible effects of precipitates and extended defects such as dislocations and grain boundaries (GBs) on bubble nucleation were ignored, i.e. it was assumed to occur homogeneously within an otherwise perfect matrix lattice. In metals and alloys for technical applications, such defects may play a crucial role in bubble nucleation, particularly in the high temperature regime where bubble densities are low.

3.4.1. Low temperatures

Dislocations, precipitate-matrix interfaces, particularly the one of incoherent type, and GBs act as strong traps for mobile He atoms. Trapping of He atoms at those sites competes with He atom clustering within the perfect lattice.

At low temperatures, where thermal dissociation from He atom traps is negligible, the globally dominant nucleation mode, homogeneous vs. heterogeneous, is determined by the relation between the partial sink strengths of bubble nuclei according to homogeneous nucleation and of pre-existing deep traps. Homogeneous nucleation will be dominant if the sink strength of bubble nuclei, i.e. the product of their density as predicted according to Eq. (2), and their size, is larger than the sink strength of other pre-existing traps, for instance the corresponding product of density and size of precipitates, and visa versa, depending on temperature and He production rate. In the latter case, for given precipitate parameters, homogeneous nucleation will be dominant at low temperature and/or high He production rates, and visa versa. Maps for homogeneous vs. heterogeneous nucleation in the presence of precipitates corresponding to these trends have been introduced previously [20].

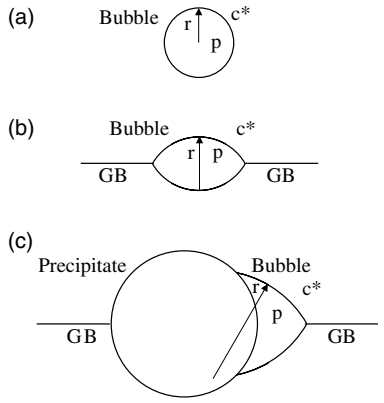

Fig. 6. Illustration of interfacial effects on cavity nucleation at high temperatures; (a) spherical nucleus in the matrix, (b) lenticular nucleus at a GB, (c) truncated lenticular nucleus at a GB-precipitate, all assumed to have the same volume. Under this condition, the radius of curvature of the nucleus surface, r, increases while the corresponding equilibrium gas pressure inside it, $p = 2\gamma/r$, and the thermal equilibrium He concentration around it, $c^*(p)$, decrease, suggesting that the critical concentration required for bubble nucleation decreases and bubble nucleation becomes easier from configuration (a) to (c).

3.4.2. High temperatures

At high temperatures, where thermal dissociation from He atom traps must be considered, the relation between the partial sink strengths of possible nucleation sites does no longer provide a sufficient criterion for homogeneous vs. heterogeneous nucleation. In this case, effects of dislocation cores, interfaces and GBs on the thermodynamics of critical bubble nuclei, more precisely on the state of He atoms in them and the corresponding thermal equilibrium He atom concentration around them, c^* (as appearing in Eq. (3)), are important.

In Fig. 6, the 'classical' understanding of these interfacial effects on the thermodynamic state of a nucleus of given volume, i.e. on the radius of curvature of its surface, r, the corresponding equilibrium gas pressure inside it, $p = 2\gamma/r$, where γ is the specific surface free energy, and the thermal equilibrium He concentration around it, $c^*(p)$, are illustrated. At given nucleus volume, interfacial equilibrium at triple junctions between surface segments of a bubble and a GB, Fig. 6(b), or, in addition, between surface segments and a precipitate-matrix interface, Fig. 6(c), results in an increase in r and corresponding decreases in $p(r)$ and $c^*(p)$. This effect increases with increasing number of interfaces involved, i.e. from the configuration of Fig. 6(b) to that of Fig. 6(c).

These relationships suggest that heterogeneous bubble nucleation at interfaces and GBs would occur at lower critical He concentration c^* than homogeneous nucleation (assuming that bubble nucleation would occur at a certain minimum critical nucleus size), and would be reached earlier therefore in the former than in the latter case. Consequently, a significant reduction of the He concentration by substantial premature heterogeneous nucleation would prevent additional homogeneous nucleation. To our knowledge, the conditions for this behaviour have not been studied systematically.

3.5. Bubble nucleation at extended defects

In the preceding section, general conditions for the global dominance of one of the two main bubble nucleation modes in a matrix containing pre-existing traps for He atoms, homogeneous vs. heterogeneous nucleation, have been discussed. The detailed evolution of bubbles at extended defects such as dislocations and GBs [12,13,21–23] is controlled by fluxes of He atoms to such sites, which constitute effective local He production rates there, and these fluxes are controlled by the bubble evolution within the bulk of the matrix as illustrated in Fig. 7. Thus, the bubble evolution at extended defects is strongly coupled to that in the bulk.

In modelling bubble nucleation at extended defects, both the flux of He atoms to them from the bulk and their diffusion along the extended defect must be considered. A detailed description of these processes is complicated. Attempts have been made to describe the main features [12,13,21–23]. A few qualitative features are worth mentioning here:

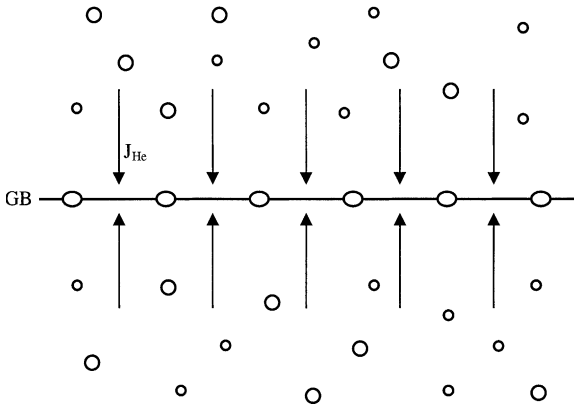

Fig. 7. Schematic illustration of He fluxes to GBs controlled by the bubble evolution within the bulk of the matrix. These constitute effective local He production rates at GBs. Thus, the bubble evolution at extended defects is strongly coupled to that in the bulk.

(1) Premature bubble nucleation at an extended defect results in a reduction in the He concentration and, by this, in a strongly reduced nucleation probability in their vicinity which manifests itself as bubble denuded zones adjacent to the extended defect.

(2) An extended defect collects a substantial fraction of the He atoms produced in such zones.

For a quantitative modelling of bubble nucleation at extended defects, an important parameter would be the diffusion constant for He diffusion along the considered extended defect which must be expected to depend significantly on the type of extended sink (dislocation or grain boundary). It has indeed been demonstrated that the large variation in density and size of bubbles at different GBs observed in Cu implanted with He at 738 K may be correlated with the varying atomistic structures of the GBs, suggesting that this structure is important for the diffusivity of He along GBs [24].

4. Bubble coarsening upon annealing

4.1. General features

In the preceding sections, bubble nucleation and growth during He production at elevated temperatures was discussed. When a metal, into which He was introduced at some temperature, is annealed without further He introduction at generally higher temperature, existing bubbles or bubbles formed at the beginning of annealing tend to coarsen at constant He content, meaning that their average size increases while their density decreases (see Fig. 3).

The commonly used experimental procedure for studying bubble evolution at a given He content is pre-implantation of He at low temperature, generally at room temperature, where the mobility of He atoms is relatively low or even negligible, and subsequent annealing at elevated temperatures where He atoms as well as bubbles are mobile and/or He atoms dissociate from bubbles. The main parameters controlling the bubble evolution in such experiments are temperature, He concentration and annealing time. The main trends observed are [11]:

(1) At a given temperature, the density of bubbles decreases while their average size increases with time (which is the meaning of 'coarsening'), in many cases starting from some unknown sub-microscopic pre-annealing state. The character of the corresponding time-dependencies (type of power law), depends on temperature, He concentration and material conditions.

(2) The temperature dependence of bubble densities exhibits two clearly discernible branches, one at low and the other at high temperature, characterised by low and high apparent activation energies, respectively, similar as for bubble formation during He production at elevated temperatures (see Fig. 2).

(3) At a given temperature and time, the density of bubbles and, under certain conditions, also their size increase with increasing He concentration, but the latter is found to be virtually independent of He concentration under other conditions, particularly in the high temperature/low He concentration range.

The latter feature can be rationalised in the following way. During pre-implantation defining the initial state of annealing, the nucleation stage, i.e. the critical He concentration, c^*, may not or may be reached depending mainly on temperature (see Section 3.2). Accordingly, significant bubble nucleation may or may not occur at the beginning of annealing. The generally short initial state of He atom clustering is, however, irrelevant for advanced stages of bubble coarsening.

4.2. Coarsening mechanisms

In bubble coarsening upon annealing two qualitatively different mechanisms as illustrated in Fig. 8 have to be distinguished:

(1) Bubble migration and coalescence (MC) [25,26], and
(2) Ostwald ripening (OR) [27,28].

Bubble migration is due to random rearrangements of the bubble surface by diffusion of matrix atoms, most likely by surface diffusion. In the latter case, the apparent activation energy of the bubble density reached during annealing is about (minus) half of the surface diffusion energy, depending somewhat on the thermodynamic state of the bubbles.

Ostwald ripening is due to thermally activated resolution from (small) and re-absorption of He atoms by

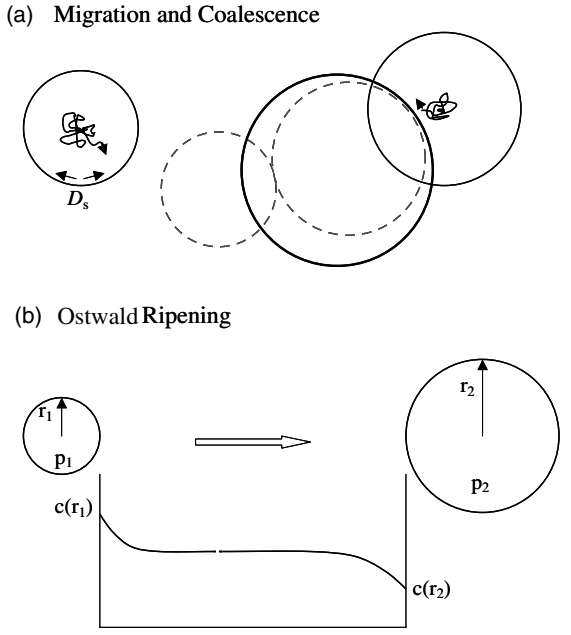

Fig. 8. Schematic illustration of the two main bubble coarsening mechanisms, (a) migration and coalescence via surface diffusion, (b) Ostwald ripening due to He fluxes driven by differences in the thermal equilibrium He concentrations in the vicinity of small and large bubbles.

(large) bubbles. This suggests that the apparent activation energy of the bubble density reached by OR is equal to the energy for He dissociation from bubbles which is significantly higher than that for MC. Accordingly, MC and OR are expected to be dominant at relatively low and high temperature (and/or high and low He concentrations), respectively.

In addition to the dissociation and re-absorption of He atoms, OR of He bubbles requires the dissociation and re-absorption of vacancies. Accordingly, this basically two-component OR process may be He atom or vacancy dissociation controlled, mainly depending on which of the two dissociation energies is higher [29].

MC vs. OR mechanism maps in space of the relevant parameters have been presented [30,31]. Such maps depend strongly upon the assumptions concerning the details in the mechanism underlying bubble migration and the activation energy for dissociation of He from bubbles.

Frequently, attempts have been made to identify the mechanism underlying an observed isothermal coarsening on the basis of the time-dependencies, for instance the exponent of a temporal power law, which does not represent, however, a reliable criterion. The strength of the temperature dependence mentioned above is a better but also not a fully reliable signature. It has been shown that the invariance of certain quantities characterising coarsening, for instance the independence of the bubble size upon the implanted He concentration in the case of OR, represent the most reliable criteria for identifying the mechanism underlying observed coarsening [20,31].

It should be noted here that bubble coarsening is substantially complicated in the presence of and close to precipitates, dislocations and GBs. Under high temperature creep, bubble sweeping by dislocation motion and GB sliding can substantially contribute to bubble coarsening [32,33].

4.3. Comparison with bubble formation during He production

The temperature dependencies of bubble densities formed in metals during annealing after He pre-implantation and those formed during He production, exhibit striking similarities, as Fig. 2(a) and (b) show for stainless steels [11]: For both types of experiments, low and high temperature branches, characterised by low and high apparent activation energies of similar magnitudes, respectively, can be clearly distinguished. The reason for this similarity is that, in both types of experiments, bubble formation is controlled by the same or similar diffusion process, He atom and/or bubble migration at low temperatures, on the one hand, and He atom or vacancy dissociation at high temperatures, on the other.

Another similarity is found when, in annealing experiments, the ratio of implanted He concentration to annealing time (upon which the bubble density is expected to depend linearly in OR) is interpreted as an effective He production rate. For the high temperature branch, normalisation of observed bubble densities, formed in stainless steels during annealing, to this effective He production rate results in a similar condensation of the widely scattered original data into a rather narrow band as for bubble densities formed during He production (Fig. 4) [11].

There is, however, a striking difference in the absolute values of the thus normalised bubble densities between the two types of experiments: they differ by about 4 orders of magnitude. This difference has been attributed to the fact that the bubble densities formed in the two cases reflect the state of He in bubble nuclei and developed bubbles, respectively, characterised by substantially different gas pressures [11]. This reasoning is, however, not fully established.

5. State of bubbles

5.1. Mechanical stability limit vs. equilibrium pressure

The state of He contained in a bubble, defined by its density (or ratio of number of He atoms to vacancies)

and the corresponding pressure, is crucial for the bubble energetics. It depends on the conditions and the stage of the bubble evolution, i.e. on temperature, He production and displacement rates, He concentration and dose, as well as bubble size. For possible values of the pressure inside a bubble, two distinctly different limiting cases represent useful guidelines:

(1) The mechanical stability limit at which the matrix would yield by spontaneous plastic deformation, most likely by dislocation loop punching. Calculations have shown that the corresponding upper bound limit of the pressure may be reasonably well represented by [34]

$$p \leqslant 0.2\mu, \tag{5}$$

where μ is the shear modulus of the matrix.

(2) The condition of thermodynamic equilibrium yields

$$p = 2\gamma/r, \tag{6}$$

where γ is the surface free energy.

At high He to dpa ratio, high He production rate and concentration, where He dominates the bubble evolution since most of the concurrently produced SIAs and vacancies are annihilated at existing bubbles, it is conceivable that the pressure is close to the limit given by Eq. (5) [34]. For Ni, and austenitic steels where $\mu \approx 90$ GPa, this limit is as high as 18 GPa.

A sufficient thermal equilibrium vacancy concentration is required to establish thermal equilibrium of bubbles according to Eq. (6) which holds around and above stage V ($T > 0.4T_m$). In small nm-scale bubbles, for instance in Ni and austenitic steels where $\gamma \approx 2$ N/m, the equilibrium pressure reaches also values in the GPa range, but clearly not as high values as those defined by the mechanical stability limit. It is emphasised here that at high He to dpa ratio and high He concentrations, the pressure remains significantly above the thermal equilibrium value even above stage V.

5.2. High density equation of state for helium

For pressures in the GPa range expected in small nm-scale bubbles or, even higher, in bubbles close to the mechanical stability limit, the equation of state (EOS) of He is neither adequately described by the ideal gas, nor by the van der Waals law, and even not by some form of the hard sphere EOS. Mills et al. [35] have provided a useful parametrisation of their experimental high pressure data. This does, however, not behave correctly at very high pressures of several GPa. A semi-empirical EOS, based on Becks potential and the use of virial expansion and quasi-harmonic approximation [20], is expected to be adequate even at pressures of tens of GPa.

5.3. Bubble to void transformation under vacancy supersaturation

At temperatures around and above stage V ($T > 0.4T_m$), an irradiation or stress induced effective vacancy supersaturation, which does not reach a sufficiently high level required for direct void nucleation, can, nevertheless, transform stable bubble type cavities, growing initially by He atom absorption at $p \approx 2\gamma/r$, into void-type cavities, growing subsequently by vacancy absorption at decreasing $p < 2\gamma/r$, when a certain critical size is reached. Formally, in cavity growth kinetics, this critical size is defined by the convergence of a stable (bubble) and an unstable point of vanishing growth (critical void nucleus). For a bubble containing ideal gas on a GB across which a mechanical tensile stress, σ, is acting, the critical radius (of curvature) of the cavity is found to be given by [12,13]

$$r^*(\sigma) = 4\gamma/3\sigma. \tag{7a}$$

When the stress is removed, the size of the critical bubble relaxes to

$$r_0^*(\sigma) \equiv r^*(\sigma = 0) = r^*(\sigma)/\sqrt{3}. \tag{7b}$$

For a bubble in the bulk of the matrix subject to an irradiation induced effective vacancy supersaturation, the stress in Eq. (7) has to be substituted by kT ln(vacancy supersaturation) where kT is the thermal energy [36,37].

6. Special bubble structures and growth mechanisms

6.1. Helium platelets

In some metals (Ti, Ni, Mo) and in all covalent materials studied so far (Si, B_4C, SiC, Al_3O_2) (for references see [38,39]), He introduction at room temperature under relatively small displacement damage was observed to result in penny-shaped He precipitates or 'He platelets'. Most pronounced and thermally very stable He platelets have been recently observed in SiC [38,39].

In the limiting case of negligible availability of intrinsic or irradiation induced mobile vacancies necessary for forming three-dimensional bubbles, an efficient way for He interstitial atoms to acquire space during clustering and to minimise by this their energy is the formation and growth of an oblate two-dimensional precipitate between two atomic layers of the matrix lattice, thus representing a growing He-filled Griffith crack. But even for a small finite number of vacancies involved in He clustering, a platelet-like structure is energetically more favourable, because of the more efficient elastic relaxation, than a spherical bubble, as long

as the number of He atoms per vacancy and the corresponding pressure are above a certain level.

Accordingly, platelet-like bubble structures generally indicate high gas pressures and, by this, a low availability of vacancies for He clustering. Assuming that observed He platelets do not contain vacancies and thus represent ideal Griffith cracks, extremely high values for the pressures of the He contained are obtained for small platelet sizes depending on the elastic strength of the matrix. For the observed crack-like He platelets in SiC, which has a very high elastic strength, a particularly high pressure of about 24 GPa is found where He is expected to be solid even up to 470 K [38,39].

In the case of SiC, the following additional puzzling experimental observations [38,39] is to be considered: Implantation of He at RT to a certain concentration (0.25%) results in the formation of He platelets with surprisingly uniform size and this size is maintained upon further He implantation and upon annealing up to about 1300 K without any indication of growth as expected for normal gas bubbles [28]. This growth limitation of He platelets in SiC has been rationalised in terms of their self-trapping by circular dislocations dipoles assumed to form close to their rim at some critical size, and to stay there at temperatures (below about 1300 K) where both dislocation glide and climb are negligible [40]. Such a temperature range does not exist in metals because of the low Peierls barrier against dislocation glide there.

6.2. Ostwald ripening of bubble–loop complexes

When SiC implanted with He is annealed at temperatures 1300 K $< T <$ 2100 K, another puzzling experimental observations has been made: The He platelets formed during RT He implantation transform to complexes of bubbles and dislocation loops of different degree of complexity which coarsen such that both components, bubbles and loops, within each complex always occupy the same, even if growing, total volumes.

This surprising feature has been rationalised in terms of a new type of Ostwald ripening process in which He atoms are transferred from small to large complexes by dissociation, long range bulk diffusion and re-absorption, as in the case of normal OR of bubbles, while matrix atom diffusion is restricted to the surfaces of bubbles and to the cores of the dislocation loops, allowing only local transfer of matrix atoms between bubbles and associated loops (see Fig. 9) [40]. Thereby, the He transfer between complexes is driven by differences in the pressures within small and large bubbles coupled to differences in the sizes of bubbles and associated loops, while matrix fluxes along the cores of the dislocation loops to or from the associated bubbles are driven by gradients in the chemical potential of the matrix atoms resulting from gradients in the local curvature of the loops. The slower of the two transfer processes is rate controlling one. Assuming that matrix atom transfer between bubbles and associated loops is the slower process, time and temperature dependencies of the average bubble and associated loop size have been derived, in good agreement with the corresponding experimental data [40].

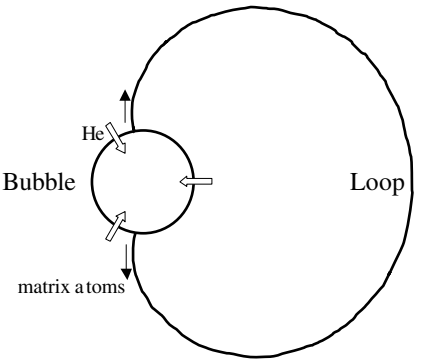

Fig. 9. Growth of a bubble–loop complexes by the absorption of He atoms from the environment and the concurrent transfer of matrix atoms to the dislocation loop. The flux of matrix atoms along the core of the dislocation loop is driven by a decrease in the chemical potential associated with a decrease in the curvature of the loop.

During the OR process, the pressure in the bubbles decreases according to the increase in the size of the complexes, but remains above the thermal equilibrium pressure defined by Eq. (6), as long as the loops are separated without forming a dislocation network. Only above about 2100 K, where bulk self-diffusion becomes substantial, the kinetic restriction of matrix atoms to surfaces and dislocation cores is relieved and OR of bubbles occurs in the normal way with pressures close to thermal equilibrium.

In metals, where the analysis of bubble coarsening at high temperatures for some cases (Ni, austenitic and martensitic steels) indicates that He dissociation from bubbles is not easier than bulk self-diffusion, there is most likely no (intermediate) temperature range where the above described coupled OR would occur, with He transfer between bubbles through the bulk and matrix atom transfer between bubbles and loops restricted to dislocation core diffusion. The latter process may, however, play a role in the He driven growth of bubbles attached to loops during He production at intermediate temperatures.

7. Helium induced hardening and embrittlement

Radiation induced changes in the mechanical behaviour of metallic materials originate in changes in the

microstructure. Accordingly, the temperature dependence of mechanical property changes induced by He reflects the temperature dependence of the bubble structure described in Section 3. We start with He induced mechanical property changes at high temperatures, $T \geqslant 0.4T_m$, where these are particularly pronounced.

7.1. High temperature embrittlement due to He

For studying high temperature embrittlement due to He, creep tests on samples performed after (low temperature) He implantation/irradiation and, even better, during He implantation/irradiation are the most instructive mechanical test modes. In both cases, in spite of distinct qualitative and quantitative differences, the main effects of He on the high temperature creep strength of metals are [3,41]:

(1) change of the fracture mode from transgranular to intergranular,
(2) reduction of the time and strain to fracture, by factors increasing with increasing test temperature and stress (or strain rate) up to several orders of magnitude, depending on the material considered.

These features have been rationalised in terms of the nucleation of He bubbles on GBs, their growth by He atom absorption or coarsening in creep tests during or after He implantation, respectively, their transformation to voids and subsequent growth under the action of a tensile stress, and their (local) coalescence resulting in crack formation and fracture [3,12,13]. The evolution of the cavity structure on GBs consists of a sequence of stages corresponding to these processes.

For cases exhibiting the above mentioned qualitative features (1) and (2), it has been shown by estimates based on TEM data of bubbles on GBs that the creep life time is dominated by the stage of growth of stable He bubbles on GBs ('gas driven' during 'in-beam'/'in-pile' tests, and coarsening controlled in tests after implantation/irradiation) from their nucleation to their transformation to void-type cavities [12,13]. This conclusion has been nicely confirmed by a series of creep tests performed at constant stress, σ, on samples pre-implanted at the test temperature to increasing He concentrations [3]. As shown in Fig. 10, the He effect remains moderate as long as the initial average radius of GB bubbles, $\bar{r}$ (monitored by TEM after He implantation into the stress-free sample), does not reach the relaxed critical radius, $r_0^*(\sigma)$, given by Eq. (7b), whereas failure occurs almost immediately after stress application when $\bar{r}$ exceeds $r_0^*(\sigma)$.

The concept of a transformation of meta-stable bubbles to unstably growing void-type cavities has been generalised to the more complicated dynamic situation

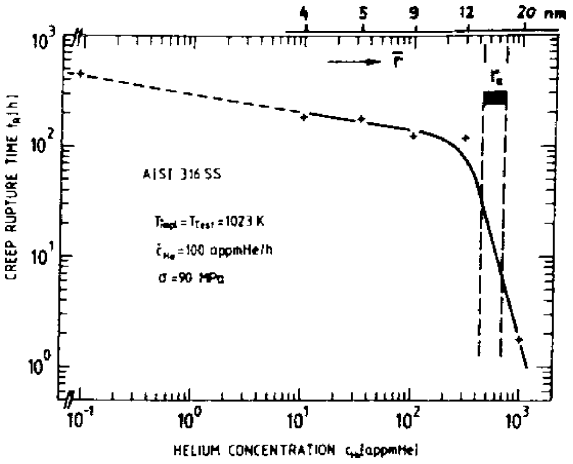

Fig. 10. Time to rupture, t_R, vs. He concentration, c_{He}, for creep tests performed at constant stress, σ, on samples pre-implanted at the test temperature. When the average radius of GB bubbles, $\bar{r}$, observed in TEM reaches the critical value $r_0^* \approx 15$ nm, t_R drops drastically (after He implantation into the stress-free sample) does not reach the relaxed critical radius, $r_0^*(\sigma)$, given by Eq. (7b), whereas failure occurs almost immediately after stress application when $\bar{r}$ exceeds $r_0^*(\sigma)$ [3].

of high temperature fatigue of samples pre-implanted with He [42]. In this case, cavities are growing and shrinking ('breathing') under cycling stress, with a 'breathing' amplitude which was shown to depend strongly on the cycling frequency, ν. Using a limiting cycle analyses [43], the critical bubble size (referred to the maximum tensile stress in the cycling period) was shown to change from small values at low ν to large values at high ν around a critical cycling frequency, ν_c, depending on stress/strain amplitude and temperature. Accordingly, the critical cavity size is reached for $\nu < \nu_c$ at shorter time and, correspondingly, at smaller numbers of cycles to failure than for $\nu > \nu_c$.

Both the predicted 'breathing' of GB cavities under cycling stress at high temperatures and the existence of a critical frequency in the frequency dependence of the number of cycles to failure [42] have been confirmed later by TEM observations and high temperature fatigue tests, respectively [44].

7.2. Low temperatures hardening and embrittlement

In contrast to its strong effect at high temperatures, the contribution of He to hardening and embrittlement is smaller and much less clear at low temperatures, $T \leqslant 0.4T_m$. For this low temperature range, tensile tests on austenitic and martensitic steels implanted with energetic He ions or irradiated with neutrons at or somewhat above room temperature indicate that [45,46]

(1) the hardening increment per dpa decreases with increasing displacement dose such that hardening tends to saturate above about 1 dpa, and
(2) the contribution of bubbles to hardening and embrittlement is negligible at low He concentrations and becomes, after He implantation, significant only above a 'critical He concentration' around 1 at%.

A recent model for cascade induced He resolution and secondary bubble nucleation [19] suggests a change from an initially very weak increase of the contribution of bubbles to hardening with increasing He concentration/dose to a significantly stronger dependence at doses above 1 dpa. According to that model, for a significant contribution of He to hardening (and embrittlement), a certain 'critical He concentration' or 'critical dose' is required depending on both the He production and the displacement rate, or, alternatively, on the He-to-dpa ratio and one of the rates. The model demonstrates that results obtained from mechanical tests after He implantation cannot be directly extrapolated to irradiation conditions of fast fission reactors, fusion reactors, and spallation neutron sources, and provides some idea how adequate extrapolations could look like. But the problem of the He contribution to low temperature hardening and embrittlement is far from having been solved.

8. Where do we stand?

As mentioned in the introduction the main concern regarding helium accumulation in metals during irradiation is the loss of ductility and the associated embrittlement. A proper treatment of the whole problem of helium induced embrittlement requires modelling of all essential processes controlling the microstructural evolution, such as diffusion of He atoms, their trapping and dissociation from other defects, bubble nucleation and growth, as well as the relation between the evolving microstructure and the changes in mechanical properties.

Judging the progress in modelling helium effects on metals certainly depends on the personal point of view, for instance on the esteem of identifying mechanisms and describing trends relative to comprehensive attempts to describe the effects quantitatively. In addition, the evaluation depends also strongly on the parameter range considered. Thus, one may say that considerable progress has been achieved over the years in identifying the main mechanisms and parameters controlling He bubble formation and the associated embrittlement in homogeneous metals with low density of extended defects at high temperatures above annealing stage V where the displacement damage effects may be neglected. This success is mainly due to simplified analytical descriptions of the underlying processes for certain extreme limiting cases. The temperature range to which it applies is, however, technologically of little interest.

But even in this high temperature range, analytical as well as numerical models are presently far from being really quantitative, i.e. they are not able to describe the details in bubble evolution and embrittlement quantitatively as a function of temperature, He production rate and He concentration. The temperature dependence of the bubble density nucleated during He production, for instance, has been crudely attributed to only one parameter which describes the thermal re-solution and re-absorption (dissociation) of He from and by critical bubble nuclei, whereby the individual contributions of He solubility and diffusivity to this parameter and the size and state of the critical nuclei remain unclear.

At lower temperatures (around and below stage V), displacement damage, generally accompanying He production, becomes increasingly more important in the microstructural evolution, particularly for relatively low ratio of the He production to the displacement rate (low He to dpa ratio), and, with this, modelling He effects becomes substantially more complicated. At temperatures close to or somewhat below stage V, some general trends in bubble nucleation and growth occurring under conditions where these processes are still dominated by He, have been recognised. But even basic details such as the He diffusion mechanism and the role of migration of He–vacancy clusters or small bubbles in bubble formation under He production as well as the resulting dependence of the bubble density on temperature and He production rate are still not fully established. Moreover, even the range in the space of the main parameters (temperature, He production and displacement rates, or one of the rates and the He to dpa ratio) where He dominance in cavity nucleation applies is not yet clear.

In metals and alloys for technological applications, lattice heterogeneities such as precipitates, dislocations and grain boundaries play an important role in bubble formation, particularly at elevated temperatures. Such effects are also only qualitatively understood. Important details, however, such as the influence of the structure of dislocations and grain boundaries on bubble formation and on He embrittlement, have not been studied systematically so far, even though some experiments demonstrate their importance.

In the technologically relevant temperature range between stage III and V, some important problems are still not properly understood. There is, for instance, clear experimental evidence for He resolution from bubbles by cascades and its relevance for the evolution of the bubble structures at high doses, but modelling of this effect is still only at an early stage. Another problem where modelling has only started is the contribution of He to low temperature hardening and embrittlement as a function of temperature, He production and displacement rates, and displacement dose level.

Systematic experiments are required to clarify some key processes. An important example is the clarification of the He diffusion mechanisms under irradiation where modelling is presently based on theoretical speculations.

Quantitative modelling of He effects in metals requires the knowledge of key input parameters such as energies of stable and unstable configurations including binding and migration energies. Presently, 'ab initio' electronic structure calculations are only able to provide values for small configurations, for instance for the binding energy of He atoms to vacancies and small vacancy clusters. For larger He–vacancy clusters, one still depends on the use of continuum approximations such as the equation of state of He and linear continuum elasticity.

Future success in modelling He effects in metals will depend on a skillful combinations of analytical and numerical treatments of the energetics and formation kinetics of helium vacancy complexes with systematic molecular dynamics and Monte Carlo simulations, and well designed single variable experiments.

References

[1] H. Ullmaier, Nucl. Fusion 24 (1984) 1039.
[2] H. Schroeder, W. Kesternich, H. Ullmaier, Nucl. Eng. Des./Fusion 2 (1985) 65.
[3] H. Ullmaier, H. Trinkaus, Mater. Sci. Forum 97–99 (1992) 451.
[4] G.W. Greenwood, A.J.E. Foreman, E.A. Rimmer, J. Nucl. Mater. 4 (1959) 305.
[5] Radiat. Eff. 78 (1983).
[6] S.E. Donnely, J.H. Evans (Eds.), NATO ASI Series, vol. 279, Plenum, New York, London, 1991.
[7] H. Ullmaier, Landolt Börnstein, Numerical Data and Functional Relationships in Science and Technology, New Series, vol. N25.
[8] N.M. Ghoniem, S. Sharafat, J.M. Williams, L.K. Mansur, J. Nucl. Mater. 117 (1983) 96.
[9] H. Trinkaus, J. Nucl. Mater. 118 (1983) 39.
[10] A.J.E. Foreman, B.N. Singh, J. Nucl. Mater. 141–143 (1986) 672.
[11] B.N. Singh, H. Trinkaus, J. Nucl. Mater. 186 (1992) 153.
[12] H. Trinkaus, J. Nucl. Mater. 133&134 (1985) 105.
[13] H. Trinkaus, Radiat. Eff. 101 (1986) 91.
[14] B.N. Singh, A.J.E. Foreman, Scr. Metall. 9 (1975) 1135.
[15] S.I. Golubov, R.E. Stoller, S.J. Zinkle, to be published.
[16] P. Dauben, R.P. Wahi, H. Wollenberger, J. Nucl. Mater. 141–143 (1986) 723.
[17] R.S. Nelson, J. Nucl. Mater. 31 (1969) 153.
[18] N.M. Ghoniem, J. Nucl. Mater. 174 (1990) 168.
[19] H. Trinkaus, J. Nucl. Mater. 318 (2003) 234.
[20] H. Trinkaus, Ref. [5], p. 189.
[21] B.N. Singh, T. Leffers, W.V. Green, M. Victoria, J. Nucl. Mater. 125 (1984) 287.
[22] B.N. Singh, A.J.E. Foreman, J. Nucl. Mater. 191–194 (1992) 1265.
[23] A.J.E. Foreman, B.N. Singh, J. Nucl. Mater. 149 (1987) 266.
[24] P.A. Thorsen, J.B. Bilde-Sörensen, B.N. Singh, Mater. Sci. Forum 207–209 (1996) 445.
[25] E.E. Gruber, J. Appl. Phys. 38 (1967) 243.
[26] P.J. Goodhew, S.K. Tyler, Proc. Roy. Soc. London A 377 (1981) 151.
[27] G.W. Greenwood, A. Boltax, J. Nucl. Mater. 5 (1962) 234.
[28] A.J. Markworth, Met. Trans. 4 (1973) 2651.
[29] H. Trinkaus, Scr. Metall. 23 (1989) 1773.
[30] P.J. Goodhew, in Ref. [6], p. 349.
[31] H. Schroeder, P. Fichtner, H. Trinkaus, in Ref. [6], p. 289.
[32] W. Beere, J. Nucl. Mater. 120 (1984) 88.
[33] A. Ryazanov, H. Trinkaus, H. Ullmaier, unpublished work.
[34] H. Trinkaus, in Ref. [6], p. 369.
[35] R.L. Mills, D.H. Liebenberg, J.C. Bronson, Phys. Rev. B 21 (1980) 5137.
[36] G.R. Odette, S.C. Langley, in: J.S. Watson, F.W. Wiffin (Eds.), Proc. Int. Conf. on Radiation Effects and Tritium Technology for Fusion Reactors, Gatlinburg, TN, 1975, vol. I, p. 395.
[37] L.K. Mansur, W.A. Coghlan, J. Nucl. Mater. 119 (1983) 1.
[38] J. Chen, P. Jung, H. Trinkaus, Phys. Rev. Lett. 82 (1999) 2709.
[39] J. Chen, P. Jung, H. Trinkaus, Phys. Rev. B 61 (2000) 12923.
[40] M. Hartmann, H. Trinkaus, Phys. Rev. Lett. (2002).
[41] H. Schroeder, P. Batfalski, J. Nucl. Mater. 117 (1983) 287.
[42] H. Trinkaus, Scr. Metall. 15 (1981) 825.
[43] H. Trinkaus, H. Ullmaier, J. Nucl. Mater. 155–157 (1988) 148.
[44] I.S. Batra, H. Ullmaier, K. Sonnenberg, J. Nucl. Mater. 116 (1983) 136.
[45] J.D. Hunn, E.H. Lee, T.S. Byun, L.K. Mansur, J. Nucl. Mater. 282 (2000) 131.
[46] H. Ullmaier, J. Chen, J. Nucl. Mater. 318 (2003) 228.